form a sharp image. The result suggests a limitation of this optic system as a whole on the tissue depth of image acquisition which was approximately a 30-μm depth from the tissue surface. Therefore microvessels and thrombi residing in the superficial layer lying no more than 30 μm from the surface were subjected to this study.

Figure 2

Thrombus formation upon laser ablation

Upon the injury by laser ablation, a thrombus started to form typically over a 20 second to 1 min period. Thereafter either did it remain rather constant in size with producing small emboli or it embolized as a whole cluster and started to form another thrombus. A small population of platelets tethering at the growing thrombus appeared to change their shape from normal discoid to flattened morphology. Figure 3 (Movie 1) shows such a process between 20 seconds and 40 seconds after the start of laser ablation. Spatial distribution of platelets in and around the thrombus was evaluated by three-dimensional reconstruction.

Figure 3 (Movie 1)

Figure 4 (Movie 2) and Figure 5 (Movie 3) are the representative three-dimensional images where the scan was made on the longitudinal or radial axis of the venule, respectively. As seen, the optical resolution of the system was sufficient to visualize the interaction between the growing thrombus and circulating platelets on this venule.

Figure 4 (Movie 2)

Figure 5 (Movie 3)

Figure 6 shows temporal changes in thrombus shape. At 0 second, the initial image showed minimal fluorescence. At 20 seconds, platelets started to accumulate on the point of injury on the vessel wall. At 26 seconds, the platelet thrombus expanded further.

Figure 6

DISCUSSION

In the present study, we established an intravital imaging system with which the platelet interaction can be visualized in real-time during thrombus formation on the mesenteric

microcirculation. The optical-and the time-resolution of the system were sufficient to visualize the interaction between the growing thrombus and circulating platelets under the current condition. Utilizing an analog camera system offers the advantage that thrombus formation is visualized on-line with high resolution. This approach therefore enabled us to obtain three-dimensional geometry of the growing thrombus and to study the kinetics of thrombus growth *in vivo*.

To examine the process of thrombus formation, assessment must be ideally performed vertically as well as horizontally through the whole volume of a thrombus. The current system enables to rapidly acquire the information for a thrombus residing in the superficial layer lying no more than 30 μm from the mesenteric surface. It could be speculated that due to the light scattering properties of the imaged tissue, confocal images often suffer from significant intensity attenuation in deeper parts of the specimen [6,7]. The reason could be that both the laser as well as the emitted light are absorbed and scattered more in deeper parts of the specimen than in parts near the objective lens. This could have caused a greater rejection of the light from the sample to form the image through an array of microlens of Nipkow spinning disk.

Despite the non-ideality of this system discussed above, the system is able to acquire high-spatial resolution images with video-frame rate that can provide us important information to analyze platelet behavior *in vivo*. As seen in Figure 3 (Movie 1), the system is capable of acquiring very sharp images of individual platelets at the site of growing thrombus. Although circulating free flow platelets were rapidly moving, time resolution appears to be appropriate to detect the behavior of tethering and/or adherent platelets of which are the majority in and around a thrombus without severe blur along the longitudinal axis of the vessel (Figure 4 and 5 (Movie 2 and 3)).

With the laser-induced injury, we observed that as soon as the endothelium was damaged by the laser, platelets rapidly started to accumulate to form a hemostatic plug which was confined at the injured site (Figure 6). Our methodology allowed us to examine process and content of growing thrombus at the sites of injured vasculature. At present, our system is equipped to capture two different fluorophores that can be excited by 488 nm and 568 nm without crossover of fluorescence. To gain the insight for the kinetics of growing thrombus, its laser source and filter systems should be developed further to visualize the components of growing thrombus other than platelets, e.g. fibrin and tissue factors, which was accomplished by the system of Falati *et al* [3]. In conclusion, the current instrumentation enables us to unravel the biological and rheological properties of single platelet behavior in and around a developing thrombus *in vivo*.

ACKNOWLEDGMENTS

This work was supported by Health Labour Sciences Research Grant, Research on Advanced Medical Technology from the Ministry of Health Labour and Welfare (to M.K.), and Grant-in-Aid for Creative Scientific Research, Leading Project for Biosimulation, the 21st Century Center-of-Excellence Program from the Ministry of Education, Culture, Sports, Science and Technology in Japan (to M.S.). Our gratitude goes to Mr. Toshihiro Ochiai who immensely helped us to make this system work.

REFERENCES

1. Arfors KE, Dhall DP, Engeset J, Hint H, Matheson NA, Tangen O. Biolaser Endothelial Trauma as a Means of Quantifying Platelet Activity in vivo. *Nature.* 1968;218:887-888.
2. oude Egbrink MG, Tangelder GJ, Slaaf DW, Reneman RS. Thromboembolic reaction following wall puncture in arterioles and venules of the rabbit mesentery. *Thromb Haemost.* 1988;59:23-28.
3. Falati S, Gross P, Merrill-Skoloff G, Furie BC, Furie B. Real-time in vivo imaging of platelets, tissue factor and fibrin during arterial thrombus formation in the mouse. *Nat Med.* 2002;8:1175-1180.
4. Katayama T, Ikeda Y, Handa M, Tamatani T, Sakamoto S, Ito M, Ishimura Y, Suematsu M. Immunoneutralization of glycoprotein Ibalpha attenuates endotoxin-induced interactions of platelets and leukocytes with rat venular endothelium in vivo. *Circ Res.* 2000;86:1031-1037.
5. Suematsu M, DeLano FA, Poole D, Engler RL, Miyasaka M, Zweifach BW, Schmid-Schonbein GW. Spatial and temporal correlation between leukocyte behavior and cell injury in postischemic rat skeletal muscle microcirculation. *Lab Invest.* 1994;70:684-695.
6. Shen CL, Scott GL, Merchant F, Murphy RM. Light scattering analysis of fibril growth from the amino-terminal fragment beta(1-28) of beta-amyloid peptide. *Biophys J.* 1993;65:2383-2395.
7. Hell S, Reiner G, Cremer C, Stelzer EHK. Aberrations in confocal fluorescence microscopy induced by mismatches in refractive index. *J Microscopy.* 1993;169:391-405.

FIGURES (7 figures including 3 movies)

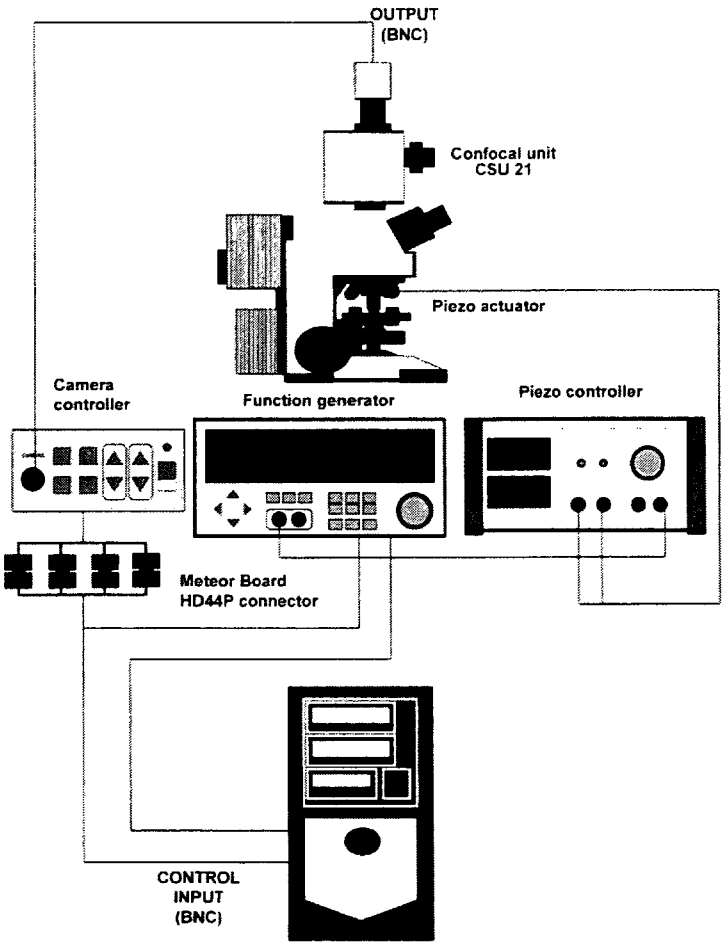

Figure 1. Schematic representation of the experimental setup. See text in Materials and Methods for details.

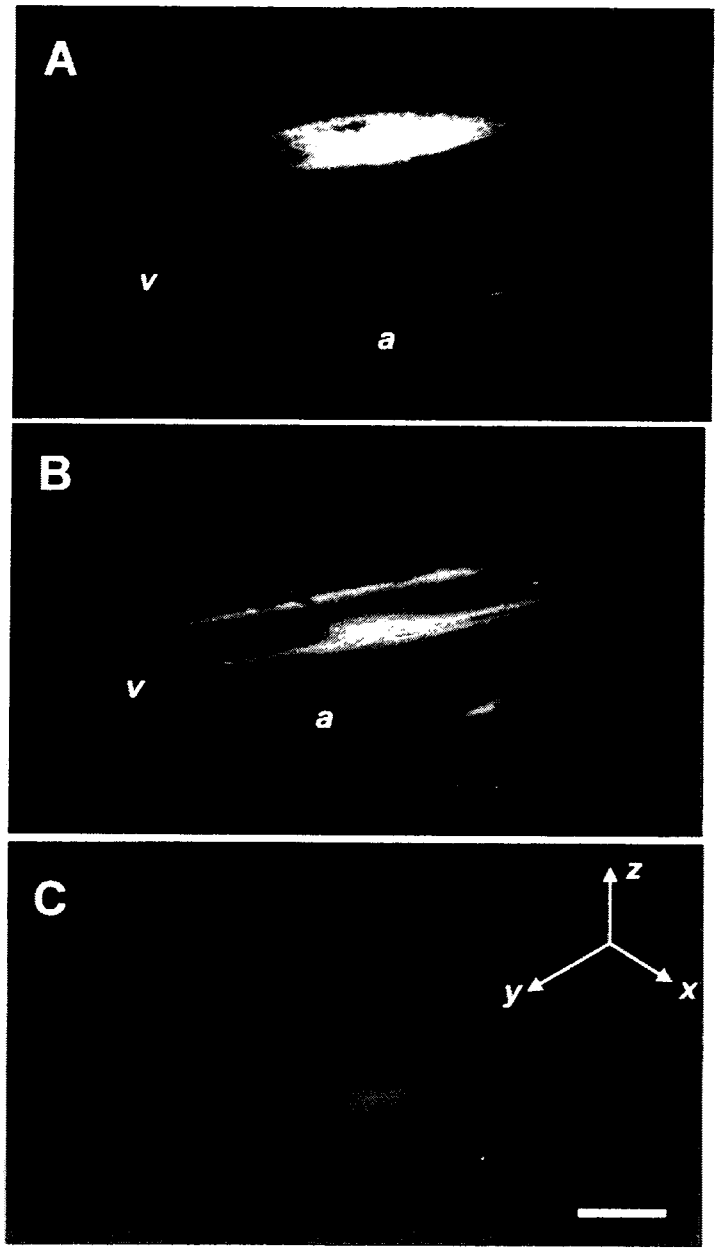

Figure 2. Three-dimensional images of CFSE-associated fluorescence at 10 min after the initial ablation of the venule. At each *x-y* confocal plane, a 2D image was obtained and these images were stacked in sequential order with an imaging-software to yield a 3D images of the rat mesentery. The image seen in panel A was reconstituted from twenty-eight different *x-y* planes covered 45-μm depth of the tissue, and each images are 1.5- μm apart. The x-y dissecting plane was moved 18.7-μm (panel B), and further 18.3-μm more deeply (panel C). Scale bar=30 μm. a, arteriole; v, venule.

Prolonged hemostatic ability of polyethylene glycol–modified polymerized albumin particles carrying fibrinogen γ-chain dodecapeptide

Yosuke Okamura, Toshinori Fujie, Hitomi Maruyama, Makoto Handa, Yasuo Ikeda, and Shinji Takeoka

BACKGROUND: Second-generation platelet (PLT) substitutes for treatment of bleeding were studied and the focus was on a dodecapeptide, HHLGGAKQAGDV (H12), which is a fibrinogen γ-chain carboxy-terminal sequence (γ 400-411) and exists only in a fibrinogen domain.

STUDY DESIGN AND METHODS: H12 was conjugated to the surface of polymerized albumin particles (polyAlb) modified with polyethylene glycol (PEG) chains to produce biocompatible particles (H12-PEG-polyAlb) that had prolonged blood circulation $t_{1/2}$ and were more stable in vitro and in vivo compared with H12-polyAlb (not modified with PEG). H12-PEG-polyAlb was administered intravenously into thrombocytopenic rats and the $t_{1/2}$ of the particles and the tail bleeding time were measured to evaluate the prolongation in the hemostatic effect.

RESULTS: H12-PEG-polyAlb particles modified with PEG prolonged the $t_{1/2}$ and maintained specific binding ability to activated PLTs. The particles dose dependently shortened the tail bleeding time of thrombocytopenic rats 6 hours after injection.

CONCLUSION: H12-PEG-polyAlb may be a suitable candidate for treatment of bleeding into thrombocytopenic patients as an alternative to PLT concentrate transfusion.

Platelet (PLT) transfusion plays an important role in the supportive therapy of thrombocytopenia caused by cancer or hematologic malignancies or in the perioperative period. The shortage of PLT concentrates, however, has always been a serious issue because of the short storage life (72 hr in Japan), insufficient donation, and the greater rate of demand than

ABBREVIATIONS: GP = glycoprotein; H12-PEG-polyAlb = polymerized albumin particles carrying H12 at the end of the polyethylene glycol chains; MALPEG-NHS = α-(3-[3-maleimido-1-oxopropyl]amino) propyl-ω-succinimidyl carboxypentyloxy polyethylene glycol; mPEG-NHS = α-methoxy-ω-succinimidyl carboxypentyloxy monofunctional PEG; PGE_1 = prostaglandin E_1; polyAlb = polymerized albumin particles; rHSA = recombinant human serum albumin.

From the Department of Applied Chemistry, Graduate School of Science and Engineering, Waseda University, Tokyo; and the Department of Internal Medicine and the Department of Transfusion Medicine & Cell Therapy, School of Medicine, Keio University, Tokyo, Japan.

Address reprint requests to: Shinji Takeoka, Department of Applied Chemistry, Graduate School of Science and Engineering, Waseda University, Tokyo 169-8555, Japan; e-mail: takeoka@waseda.jp.

This work was supported in part by Health and Labor Sciences Research Grants (Research on Pharmaceutical and Medical Safety, ST, MH, and YI); Ministry of Health, Labor and Welfare, Japan, and grants-in-aid from the JSPS, Japan (No. 15300171, ST); Ministry of Education, Culture, Sports, Science and Technology (Leading Project for Biosimulation, MH); and 21COE "Practical Nano-Chemistry" and "Consolidated Research Institute for Advanced Science and Medical Care" from MEXT (ST), Japan. YO was the recipient of a Research Fellowship from the JSPS for Young Scientists.

Received for publication October 6, 2006; revision received December 25, 2006, and accepted January 2, 2007.

doi: 10.1111/j.1537-2995.2007.01265.x

TRANSFUSION 2007;47:1254-1262.

supply. Furthermore, the risk of viral and bacterial infections associated with transfusion is also a serious issue. For these reasons, a number of trials have been conducted to develop PLT substitutes (artificial PLTs) reproducing PLT functions such as tethering and adhesion, or enhancing the hemostatic ability,[1] such as infusible PLT membranes,[2] solubilized PLT membrane protein–conjugated liposomes (plateletsome),[3] fibrinogen-bonded red blood cells (RBCs),[4] fibrinogen-coated albumin microcapsules (synthocyte),[5] liposomes bearing fibrinogen,[6] and arginine-glycine-asparaginic acid (RGD) peptide-bound RBCs (thromboerythrocytes).[7] These PLT substitutes consist of materials derived from blood components.

Glycoprotein (GP) IIb/IIIa, which exists on the PLT membrane, changes from an inactive form to an active form when PLTs adhere to a collagen-immobilized surface.[8-10] The activated GPIIb/IIIa acts as a receptor for fibrinogen and von Willebrand factor,[11-13] followed by PLT aggregation.[14,15] This is because fibrinogen contains three putative binding sites to GPIIb/IIIa, namely, a tetrapeptide containing an RGD sequence, for example, RGDF and RGDS at α95-98 and α572-575, respectively, and a dodecapeptide (HHLGGAKQAGDV, H12) at a α-chain carboxy-terminal segment (α400-411).[16]

To prepare the PLT substitutes enhancing the hemostatic ability, we also conjugated fibrinogen[17] to biocompatible carriers such as polymerized albumin particles (polyAlb)[18,19] and phospholipid vesicles (liposomes).[20-24] These fibrinogen conjugates were shown to facilitate PLT aggregation on an activated PLT-immobilized surface in vitro by recruitment of the flowing PLTs in the aggregates after their attachment.[17] Fibrinogen isolated from human plasma, however, is not stable[17] and tends to precipitate at 4°C within a few hours.[25]

Therefore, we focused on a stable dodecapeptide (H12) instead of fibrinogen.[16,26-29] Based on our results obtained from the flow cytometric analyses of PLT agglutination, the H12 conjugates showed minimal interaction with nonactivated PLTs compared with RGD conjugates.[30] Furthermore, the H12-conjugated polyAlb enhanced the in vitro thrombus formation on a collagen-immobilized plate when exposed to the flowing thrombocytopenia imitation blood.[31] When we measured the tail bleeding time at 5 minutes after the injection of the H12-polyAlb, we found a dose-dependent reduction in the bleeding time. The H12-polyAlb was of limited use, however, because the $t_{1/2}$ of the H12-polyAlb was extremely short (approximately 10 min).[31]

Polyethylene glycol (PEG) modification on the surface of carriers such as phospholipid vesicles or biocompatible polymeric particles has been widely used to prolong the $t_{1/2}$ or to stabilize their dispersion states.[32-35] We previously reported that PEG modification of the vesicles was effective in preventing intervesicular access and aggregation with a capillary viscosimeter and an optical microscope. Also, subcutaneous microvascular studies showed that the PEG conjugates significantly improved microcirculation (flow rate, functional capillary density, and vessel diameter).[24,32,33]

Our purpose was to produce a PLT substitute enhancing the hemostatic ability for the treatment of bleeding. In this study, we prepared polyAlb particles carrying H12 at the end of the PEG chains (H12-PEG-polyAlb) to prolong their $t_{1/2}$ and to enhance their stability in vitro and in vivo. The H12-PEG-polyAlb particles were intravenously administered into thrombocytopenic rats, and the tail bleeding time and the blood circulation $t_{1/2}$ were measured for evaluation of the increased hemostatic effect.

MATERIALS AND METHODS

Reagents

Fibrinogen γ-chain dodecapeptide (C-HHLGGAKQAGDV, H12) was synthesized with a solid-phase synthesizer by BEX (Tokyo, Japan). Two kinds of PEG, namely, α-(3-[3-maleimido-1-oxopropyl]amino) propyl-ω-succinimidyl carboxypentyloxy PEG (MALPEG-NHS, MW 5.0 kDa), and α-methoxy-ω-succinimidyl carboxypentyloxy monofunctional PEG (mPEG-NHS, MW 5.0 kDa), were purchased from NOF (Tokyo, Japan). Prostaglandin E_1 (PGE_1), busulfan, and PEG (mean molecular weight, 400 Da) were obtained from Sigma-Aldrich (St Louis, MO). PAC-1 and mouse immunoglobulin M (IgM) were obtained from Becton Dickinson (San Jose, CA). Fluorescein-4-isothiocyanate (FITC) was purchased from Dojindo Laboratories (Kumamoto, Japan). Recombinant human serum albumin (rHSA) was donated by Mitsubishi Pharma (Osaka, Japan).

Preparation of polyAlb

A solution of rHSA (250 mg/mL) was dialyzed against distilled water for 6 hours at 4°C to remove stabilizers such as *N*-acetyl-D,L-tryptophan and sodium caproate. The rHSA solution (200 mL) was diluted with saline to 10 mg per mL and the pH was adjusted to 10.7 (at room temperature) by titration with 0.1 N NaOH (6.4 mL). The solution was heated at 80°C for 10 minutes and rapidly cooled in an ice bath and then brought to room temperature The pH was adjusted to 6.1 at room temperature by dropwise addition of 0.1 N HCl (7.2 mL). The solution was then stirred at 40°C for approximately 120 minutes until the turbidity reached 0.4 ± 0.02. Excess iodoacetamide (25 mg) was added to terminate polymerization, and the solution was dialyzed against phosphate-buffered saline (PBS, pH 7.4) at 4°C for 24 hours. The polyAlb suspension (213 mL) was centrifuged and washed with PBS (30,000 × *g*, 10 min, 4°C) to separate the rHSA oligomers. The resultant preparation was the purified polyAlb ([rHSA] = 20 mg/mL, 30 mL). A

mean particle diameter was determined by a dynamic scattering method (Coulter N4 Plus submicron particle sizer. Beckman-Coulter, Miami, FL).

PEG modification with the surface of polyAlb carrying H12

A solution of MALPEG-NHS in dimethyl sulfoxide (DMSO; 10 mmol/L, 284 μL) was added to the polyAlb suspension (20 mg/mL [300 μmol/L], 30 mL), and the suspension was stirred for 20 minutes at room temperature. Different volumes of a 25 mmol per L solution of mPEG-NHS in DMSO (0, 284, 1136, 1704, and 2840 μL) were added to aliquots of this suspension, and the suspensions were stirred for 20 minutes at room temperature. The unreacted reagents and the by-products were separated by repeated centrifugation and washing with PBS (30,000 × *g*, 10 min, 4°C) and MALPEG- and mPEG-modified polyAlb ((MALPEG)(mPEG)polyAlb) were collected. A suspension of (MALPEG)(mPEG)polyAlb (20 mg/mL, 20 mL) was mixed with a solution of H12 (100 mmol/L, 19 μL) and allowed to react at room temperature for 12 hours. A small molar excess of cysteine over MALPEG was added to the suspension, and the unreacted reagents were removed by repeated centrifugation and washing with PBS (30,000 × *g*, 10 min, 4°C) to obtain the purified (MALPEG)(mPEG) polyAlb carrying H12 (H12-PEG-polyAlb, 10 mg/mL, 30 mL). Similarly, FITC-labeled H12-PEG-polyAlb was prepared as follows: a solution of FITC was added to the (MALPEG)(mPEG)polyAlb suspension before H12 conjugation and stirred for 20 minutes at room temperature. The unreacted FITC and the by-products were separated at the same time during separation of unreacted PEG.

The concentrations of the MALPEG, mPEG, and H12 conjugated to the surface of polyAlb were determined by the quantification of each unreacted reagent with high-pressure liquid chromatography on a TSK-GEL G3000PW$_{XL}$ column (7.8 mm o.d. × 300 mm hr with a mobile phase of 36% acetonitrile and 0.1% trifluoroacetic acid at 1 mL/min). Unreacted reagents were detected with a reflective index detector. H12-polyAlb particles to which H12 was directly conjugated were prepared with a cross-linker; *N*-succinimidyl 3-(2-pyridyldithio) propionate as described previously.[31]

Flow cytometric analyses

Blood withdrawn from healthy volunteers was mixed with 10 percent volume of 3.8 percent (wt/vol) sodium citrate. PLT-rich plasma was prepared by centrifugation (100 × *g*, 15 min, 22°C). PLT-rich plasma was mixed with a 15 percent (vol/vol) acid-citrate-dextrose (ACD) solution composed of 2.2 percent (wt/vol) sodium citrate, 0.8 percent (wt/vol) citric acid, and 2.2 percent (wt/vol) glucose (ACD) containing 1 μmol per L PGE_1. The suspension was centrifuged (2200 × *g*, 10 min, 22°C), and the plasma was replaced with a Ringer's-citrate-dextrose solution (composition, 0.76% [wt/vol] citric acid, 0.090% [wt/vol] glucose, 0.043% [wt/vol] $MgCl_2$, 0.038% [wt/vol] KCl, 0.60% [wt/vol] NaCl, pH 6.5) containing 1 μmol per L PGE_1. After the pellets were resuspended in the Ringer's-citrate-dextrose solution, the suspension was centrifuged (2200 × *g*, 10 min, 22°C), and the concentrated PLTs were resuspended at 100×10^3 per μL in a Hepes-Tyrode buffer (pH 7.4). The PLT counts were determined with an automated hematology analyzer (K-4500, Sysmex, Kobe, Japan).

The suspension of the FITC-labeled H12-PEG-polyAlb (14 mg/mL, 20 μL) was added to the PLT suspension ([PLT] = 100×10^3/μL, 50 μL) in the presence or absence of PAC-1 (approx. 0.5 μg). Thrombin (final concentration, 3 U/mL) was added to the suspension to activate the PLTs at 37°C for 10 minutes before fixing with formaldehyde (final concentration, 1.5% [vol/vol]). We carried out the same experiments for control PEG-polyAlb, H12-polyAlb, and polyAlb. The PLTs were gated to their characteristic forward versus side scatter, and 20,000 PLTs were analyzed with a flow cytometer (FACSCalibur, Nihon Becton Dickinson, Tokyo, Japan). The PLTs binding with the H12-PEG-polyAlb was quantified as a fraction of the fluorescent-positive PLTs. Each experiment was performed at least three times.

Measurement of tail bleeding time and $t_{1/2}$ of H12-PEG-polyAlb with thrombocytopenic rats

All animal studies were approved by the Animal Subject Committee of Keio University, School of Medicine, and performed according to NIH guidelines for the care and use of laboratory animals. Busulfan-induced thrombocytopenic rats were prepared as described previously.[31] A busulfan solution was prepared at a final concentration of 5 mg per mL in PEG (mean molecular weight, 400).[31] Male Wistar rats (230-250 g, CLEA Japan, Tokyo, Japan) were anesthetized with diethyl ether and injected on Days 0 and 3 with 10 mg per kg on each dosing day to produce a total dosage of 20 mg per kg busulfan. On Day 10, thrombocytopenic rats were anesthetized with sevofrane, and the sample suspension was infused into the tail vein. The samples were H12-PEG-polyAlb and PEG-polyAlb at a dose of 4 mL per kg: saline was used to obtain the control value. Several hours after administration, a 2.5-mm (length) × 1.0-mm (depth) template-guided incision (Quikheel, Becton-Dickinson) was made 1 cm from the tip of the tail. A tail was immersed in a 50-mL cylinder of saline, and the time taken for bleeding to stop was measured.

The blood circulation $t_{1/2}$ was measured from the clearance curve as follows: FITC-labeled H12-PEG-polyAlb suspension was infused into the tail vein at a dose

of 40 mg per kg (equivalent rHSA concentration). After this, 400 µL of blood was collected from the tail vein of the rats at time intervals with a 25-gauge needle and centrifuged (2200 × *g*, 10 min, 22°C), and 200 µL of plasma containing the polyAlb was collected. The plasma was mixed with a solution of 0.1 N NaOH and incubated at room temperature for 20 min to dissolve H12-PEG-polyAlb. The fluorescent intensity was then measured (E_x = 495 nm, E_m = 510 nm), and the $t_{1/2}$ was calculated with a spectrofluorometer (FP-750, JASCO, Tokyo, Japan).

Statistical analyses

Significance of data for H12-PEG-polyAlb group versus PEG-polyAlb and saline groups was tested with Tukey-Kramer tests (Fig. 3). Significance of data for H12-PEG-polyAlb group versus saline group was tested with a t test (Fig. 4). A p value of less than 0.05 was considered to be significant. Statistical analyses were performed with computer software (StatView, SAS Institute, Cary, NC).

RESULTS

Characterization of H12-PEG-polyAlb

We selected two kinds of PEG reagents; the minimum amount of bifunctional PEG (MALPEG) was used to chemically bond H12 having a mercapto group at the C-terminus, whereas mPEG was used to stabilize dispersion states of polyAlb and do not react with H12. We modified the surface of polyAlb (diameter of 200 ± 80 nm) with MALPEG to the particles. The number of molecules of MALPEG that chemically bound with one polyAlb particle was estimated to approximately 12×10^3 molecules. When the concentration of mPEG added to the MALPEG-polyAlb was 0.78, 3.1, 4.7, and 7.8 mol per mol (mole equivalent of rHSA concentration), the amount of reacted mPEG was found to be 0.35, 0.94, 1.2, and 1.2 mol per mol, respectively. The reaction was saturated at 1.2 mol per mol when the ratio of mPEG to polyAlb was 4.7 mol per mol (Fig. 1). The number of molecules of mPEG attached to one MALPEG-polyAlb particle was estimated to be approximately 18×10^3, 48×10^3, 61×10^3, and 61×10^3 molecules, respectively. The endotoxin concentration in the suspension of H12-PEG-polyAlb was below 0.25 EU per mL.

$T_{1/2}$ of H12-PEG-polyAlb

When we administrated FITC-labeled PEG-polyAlb with various numbers of mPEG modification as described above into thrombocytopenic rats, the $t_{1/2}$ of the particles significantly increased with increasing amount of bound mPEG (Fig. 1). Especially in the case of PEG-polyAlb particles with maximum mPEG modification (61×10^3 molecules), the $t_{1/2}$ of the PEG-polyAlb was estimated to be approximately 188 minutes from the clearance curve, whereas that of the bare unmodified polyAlb was estimated to be approximately 10 minutes (data not shown). Thus, we succeeded in prolonging the $t_{1/2}$ of the polyAlb almost 19-fold by PEG modification.

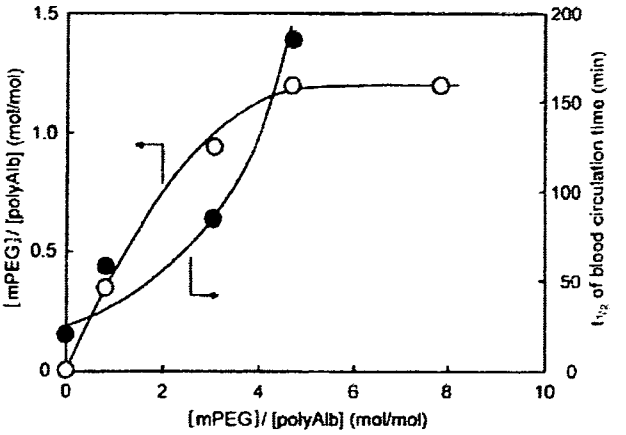

Fig. 1. Correlation of the amount of mPEG conjugated to the polyAlb (○) with blood circulation $t_{1/2}$ (●).

Flow cytometric analyses

When the FITC-labeled H12-PEG-polyAlb was added to the thrombin-stimulated PLT suspension, 86.8 ± 2.2 percent of the PLTs were fluorescently labeled (Fig. 2). In the case of nonstimulated PLTs, the ratio was 1.4 ± 0.3 percent. In the presence of PAC-1, which recognizes an epitope on the GPIIb/IIIa complex of activated PLTs at or near the PLT fibrinogen receptor,[36] the binding of H12-PEG-polyAlb to the stimulated PLTs was significantly inhibited and only 7.3 ± 0.9 percent were fluorescently labeled. The binding was not inhibited in the presence of IgM, which is an isotype-matched negative control immunoglobulin for PAC-1; in this case, 87.0 ± 3.7 percent of the PLTs were fluorescently labeled. The control PEG-polyAlb did not bind to stimulated PLTs. In the case of the H12-polyAlb (not modified with PEG), the ratio of fluorescent-positive PLTs was 91.1 ± 7.9 percent and almost equal to that found with H12-PEG-polyAlb, whereas the bare polyAlb did not show appreciable binding (1.7 ± 0.5%).

Hemostatic effects at 3 hours after H12-PEG-polyAlb administration

The tail bleeding times of the normal rats (PLT count, $810 \times 10^3 \pm 80 \times 10^3/\mu L$) and the thrombocytopenic rats (PLT count, $190 \times 10^3 \pm 20 \times 10^3/\mu L$) at 3 hours after the intravenous (IV) administration of saline were 202 ± 51 and 712 ± 131 seconds, respectively (Fig. 3). The bleeding

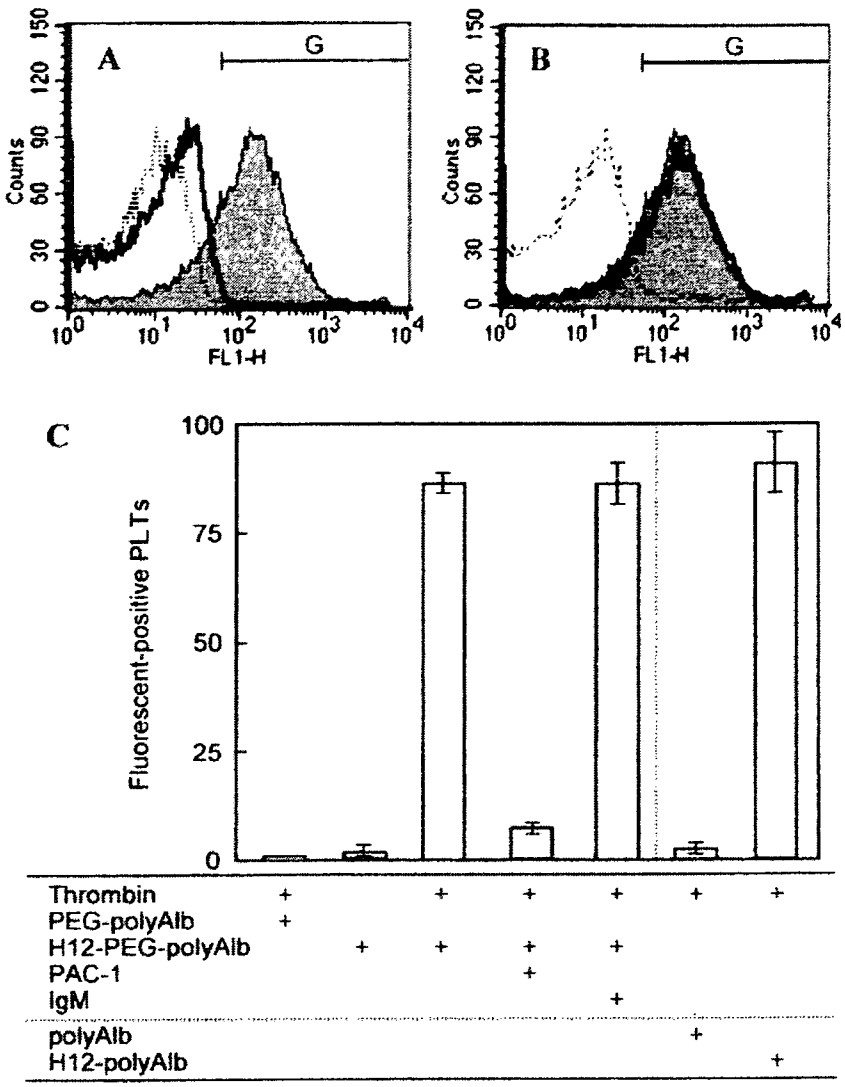

Fig. 2. Specific interactions of H12-PEG-polyAlb with thrombin-stimulated PLTs with flow cytometry. (A) The solid histogram represents thrombin-stimulated PLTs stained with FITC-labeled H12-PEG-polyAlb, the dotted histogram represents thrombin-stimulated PLTs stained with FITC-labeled control PEG-polyAlb, and the open histogram represents thrombin-stimulated PLTs stained with FITC-labeled H12-PEG-polyAlb in the presence of PAC-1. (B) The solid histogram represents thrombin-stimulated PLTs stained with FITC-labeled H12-PEG-polyAlb, the open histogram represents thrombin-stimulated PLTs stained with FITC-labeled H12-polyAlb, and the dotted histogram represents thrombin-stimulated PLTs stained with FITC-labeled control polyAlb. (C) The bar graph form was summarized in triplicate and the percentage fluorescent positive PLTs were quantified as a fraction "G" as shown in A and B.

time of the thrombocytopenic rats was approximately 3.5 times longer than that of the normal rats, suggesting that it was possible to evaluate the hemostatic effect of the H12-PEG-polyAlb in vivo with thrombocytopenic rats.

The bleeding times of the thrombocytopenic rats at 3 hours after the IV administration of the H12-polyAlb or the control polyAlb at a dose of 40 mg per kg were 590 ± 201 and 700 ± 73 seconds, respectively, and the bleeding time was almost comparable to that obtained with the control rats injected with saline. IV administration of the H12-PEG-polyAlb at a dose of 4 mg per kg did not reduce the bleeding time to 626 ± 158 seconds. For the same dose, the bleeding time of the control PEG-polyAlb group was 696 ± 108 seconds. At doses of 20 and 40 mg per kg, there was a dose-dependent reduction in the bleeding time of H12-PEG-polyAlb (Fig. 3); the bleeding times were reduced to 594 ± 184 and 330 ± 73 seconds, respectively. In comparison, the bleeding times of the control PEG-polyAlb groups at doses of 20 and 40 mg per kg were 766 ± 161 and 623 ± 99 seconds, respectively. At the dose of 40 mg per kg, the H12-PEG-polyAlb significantly reduced the bleeding time in comparison with controls.

Prolongation of hemostatic ability

The tail bleeding time of the thrombocytopenic rats before administration of H12-PEG-polyAlb or saline was 624 ± 175 seconds. The bleeding times at 5, 60, 180, and 360 minutes after administration of H12-PEG-polyAlb at a dose of 40 mg per kg were significantly reduced to 354 ± 67, 395 ± 75, 330 ± 73, and 371 ± 47 seconds, respectively, compared with that of the saline group at the same timing intervals (687 ± 131, 671 ± 142, 712 ± 113, and 538 ± 115 sec, respectively) (Fig. 4). This effect lasted for at least 6 hours. At 12 hours after administration, the bleeding time was 683 ± 149 seconds and was not significantly different from that of the saline group (890 ± 384 sec).

DISCUSSION

We previously measured the tail bleeding time at 5 minutes after the injection of H12-polyAlb, and confirmed a dose-dependent reduction in the bleeding time.[31] We then also confirmed that the $t_{1/2}$ of the H12-polyAlb was estimated to be approximately 10 minutes. The data suggested that the H12-polyAlb was of limited use because the $t_{1/2}$ of the particles was extremely short.[31]

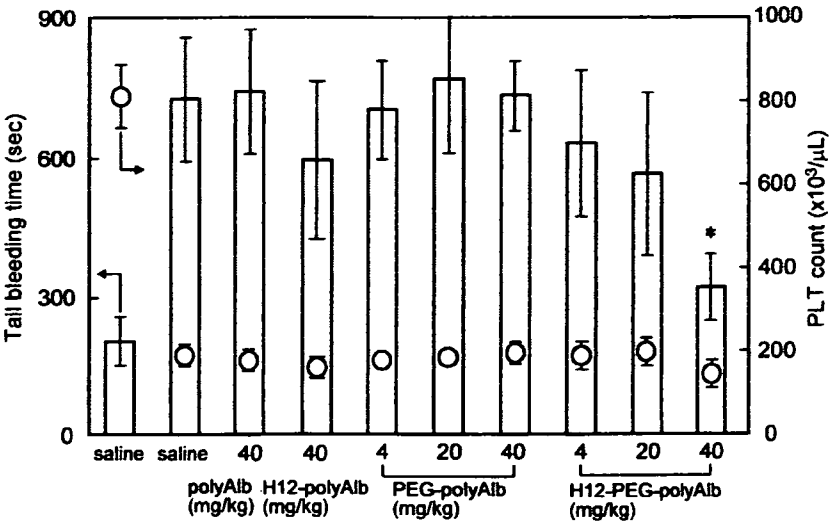

Fig. 3. Effects of the administration of H12-PEG-polyAlb on tail bleeding time at 180 minutes after injection (white bars). The administered amounts of H12-PEG-polyAlb was 4, 20, and 40 mg per kg equivalent of rHSA. (○) PLT concentration in the rats (n = 6-10). *p < 0.05 for H12-PEG-polyAlb versus PEG-polyAlb group at the same dose.

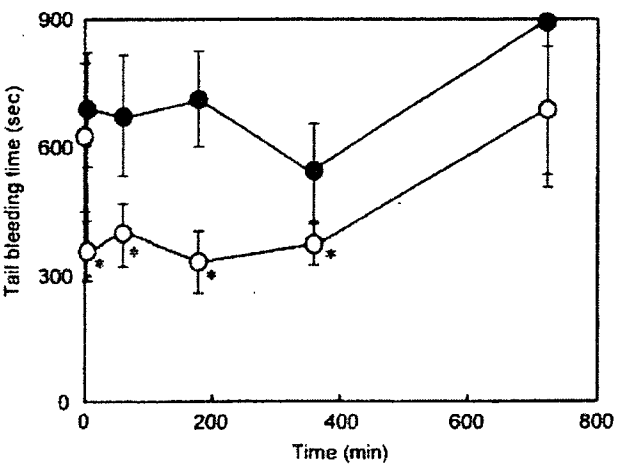

Fig. 4. Prolongation effect of hemostatic ability of H12-PEG-polyAlb on tail bleeding time (n = 5-8). H12-PEG-polyAlb (○) at 40 mg per kg equivalent of rHSA and saline (●) were administered, and tail bleeding time was measured at various time intervals after injection. *p < 0.05 for H12-PEG-polyAlb versus saline group at the same time intervals.

As noted in the introduction, PEG modification of intravenously injectable carriers has been widely used to prolong the $t_{1/2}$ or to stabilize their dispersion states.[32,33] We prepared polyAlb carrying both H12 and PEG chains to improve their stability for use in hemostasis as practical PLT substitutes.

The amount of the mPEG modifying the polyAlb increased with increasing addition of mPEG to the reaction mixture and reached saturation (Fig. 1), suggesting that PEG chains completely covered the surface of the polyAlb. The density of PEG on the particles, however, could be limited by the excluded volume effect of the neighboring PEG chains. For PEG of molecular weight 5.0 kDa, the excluded volume of the PEG chain can be estimated assuming a globular polymer chain to be of a diameter of 6.2 nm[37] If MALPEG and mPEG chains are considered to take a globular structure, which is a so-called mushroom structure, on the surface of polyAlb with a diameter of 200 ± 80 nm, the maximum number of PEG chains is estimated to 1.1×10^3. In the case of maximum PEG modification, however, the total number of PEG chains was estimated to 73×10^3, suggesting that MALPEG and mPEG chains likely take a so-called brush structure. This view was supported by results of other experiments which are briefly described below (data not shown). We used MALPEG with a molecular weight of 3.4 kDa instead of 5.0 kDa for modification of polyAlb, and modified mPEG (5.0 kDa), and then bound H12 to MALPEG modifying with the polyAlb to prepare H12-PEG-polyAlb. The modification number of mPEG increased with increasing addition of mPEG to the polyAlb, and for various preparations the number of the mPEG molecules per MALPEG-polyAlb particle was estimated to be approximately 13×10^3, 52×10^3, 78×10^3, and 112×10^3 molecules. The H12-PEG-polyAlb enhanced the ADP-induced PLT aggregation up to mPEG modification number of 52×10^3, indicating that the polyAlb cross-linked the activated PLTs to enhance the PLT aggregation. In the case of mPEG modification number of 78×10^3 or greater, however, the enhancement effect was significantly decreased, suggesting that MALPEG and mPEG chains were taking the so-called brush structure. In this structural arrangement, the functional interaction of H12 at the end of the MALPEG would be shielded because of the excluded volume effect of the neighboring mPEG chains, therefore contributing to the diminished effect of PLT aggregation with the highly modified particles noted above.

Furthermore, the conjugation number of H12 at the end of MALPEG was estimated to be approximately 10×10^3 at a yield of 52 percent, indicating that the maleimido groups of the MALPEG were exposed on the surface of the mPEG brush structures on the polyAlb. The conjugation density on the polyAlb surfaces was similar to that of H12-polyAlb which was shown to enhance PLT thrombus formation.[31] Also, the endotoxin concentration

in the H12-PEG-polyAlb was acceptable for the in vivo study.

The PEG-polyAlb tended to prolong the blood circulation time of the particles with increasing modification amount of mPEG (Fig. 1). Especially, in the case of maximum mPEG modification, the amount of FITC-labeled PEG-polyAlb at a dose of 40 mg per kg gradually decreased to 91, 89, 75, 58, 57, and 54 percent after 10, 15, 30, 60, 120, and 180 minutes, respectively (taken as 100% just after injection). Consequently, we confirmed that the $t_{1/2}$ of the PEG-polyAlb was approximately 20-fold longer than that of the bare polyAlb due to the effect of PEG modification, suggesting that the PEG-polyAlb was likely to be useful for prophylactic transfusion. Sou and coworkers[38] previously reported the circulation kinetics of phospholipid vesicles at a dose of 14 mL per kg when infused into rats and rabbits. The $t_{1/2}$ of the vesicles in rabbits was approximately twofold longer than that in rats and estimated to be equal to that in humans. This inference was based on the biodistribution of the injected particles into various organs in which the balance between organ weight and body weight is a fundamental factor determining the pharmacokinetics of the vesicles.[38] We expected that the absolute $t_{1/2}$ of the H12-PEG-polyAlb in humans was estimated to be 6 hours, and the particles may be useful as prophylactic transfusions. We are now studying the $t_{1/2}$ and hemostatic effects of the H12-PEG-polyAlb using rabbits with severe thrombocytopenia.

It is possible that the excluded volume effect of the neighboring PEG chains could shield the recognition site of H12. Therefore, we used flow cytometry to determine whether the H12-PEG-polyAlb maintained the binding ability toward thrombin-stimulated PLTs even if the polyAlb was modified with PEG chains. We found that the H12-PEG-polyAlb bound extensively to the thrombin-stimulated PLTs, whereas it did not bind to resting PLT as well as the H12-polyAlb[31] (Fig. 2). From a viewpoint of side effects, it is very important for the H12-PEG-polyAlb to interact with only the activated PLTs and not to interact with resting PLTs because of acceleration of pathologic thrombosis in the bloodstream. The binding of the H12-PEG-polyAlb to the stimulated PLTs was significantly inhibited by PAC-1, indicating that the H12-PEG-polyAlb specifically bound to the activated GPIIb/IIIa on the surface of the PLTs via H12 conjugated to the end of the PEG chain. Furthermore, we confirmed that the binding ability of the H12-PEG-polyAlb was equal to that of the H12-polyAlb.[31] It was therefore expected that H12-PEG-polyAlb may also have a hemostatic effect as well as H12-polyAlb after PEG modification.

Finally, we evaluated the hemostatic property of the H12-PEG-polyAlb with thrombocytopenic rats. In our previous studies, we succeeded in preparing thrombocytopenic rats by busulfan administration and obtaining the extinction curve of PLTs reproducibly.[31] Using hematologic indices, we determined that the concentration of busulfan, at which the PLT counts were sufficiently decreased and the RBC and white blood cell counts were maintained, was 20 mg per kg for 8-week-old rats. We further determined that the best day for the incision of the tail was Day 10 after busulfan infusion. From our previous study, the bleeding time was confirmed to correlate with PLT counts of the rats.[31]

We confirmed the dose-dependent nature of the hemostatic effect of the H12-PEG-polyAlb in vivo with moderately thrombocytopenic rats at 3 hours after infusion of the particles, suggesting that the polyAlb may be a promising candidate for a PLT substitute (Fig. 3). Based on our previous studies of latex beads carrying H12 and analyses of PLT aggregation under flow conditions with a scanning electron microscope,[30] we considered that the enhancing mechanism of H12-PEG-polyAlb was similar to that of the latex beads carrying H12 for the following reasons: 1) the adhesion of the H12-PEG-polyAlb could be initiated by the activated PLTs, which had already adhered on the surface of the exposed collagen at the vascular injury; 2) the H12-PEG-polyAlb adhering to the surface of the PLT could act as binding sites for the activated PLTs; and 3) the H12-PEG-polyAlb could accelerate the formation of the thrombus of the flowing PLTs in the thrombocytopenic blood. In contrast, the H12-polyAlb (not modified with PEG), which had a measurable hemostatic effect at 5 minutes after IV administration in our previous study,[31] did not reduce the bleeding time at 3 hours. Furthermore, we estimated the hemostatic capacity of the H12-PEG-polyAlb in comparison with PLT based on particle number. The particle number of the H12-PEG-polyAlb at a dose of 40 mg per kg was estimated to approximately 900×10^9 particles at 3 hours after IV administration. The bleeding time of the H12-PEG-polyAlb (330 ± 73 sec) was similar to that of the rats at a PLT number of approximately 10×10^9, based on the relationship between the bleeding time of the thrombocytopenic rats and PLT count.[31] This indicated that the H12-PEG-polyAlb was easy to adhere to the activated PLTs and aggregate with the PLTs on the vascular injury because the amount of H12 conjugated to the surface of polyAlb was relatively abundant. Furthermore, we also confirmed that hematologic indices did not change before and after the infusion of the H12-PEG-polyAlb. Furthermore, we confirmed that the hemostatic effect of the H12-PEG-polyAlb at a dose of 40 mg per kg lasted for at least 6 hours; however, at 12 hours after infusion, the tail bleeding time was comparable to that of the saline group, suggesting that the tail bleeding time correlated with the $t_{1/2}$ of H12-PEG-polyAlb and that the circulating H12-PEG-polyAlb may remain hardly in the bloodstream at 12 hours.

In conclusion, we succeeded in prolongation of the in vivo $t_{1/2}$ of H12-conjugated polyAlb by PEG modification (H12-PEG-polyAlb) and confirmed that the H12-PEG-polyAlb maintained specific binding ability to activated PLTs. Furthermore, the H12-PEG-polyAlb dose dependently shortened the tail bleeding time of thrombocytopenic rats and the hemostatic effects lasted for at least 6 hours. Thus, the H12-PEG-polyAlb may be a suitable candidate for an alternative to human PLT concentrates infused into thrombocytopenic patients for the treatment of bleeding. In our future prospects, we are planning to assess the hemostatic ability of the H12-PEG-polyAlb during surgery on the animals with severe thrombocytopenia and to study the safety of the H12-PEG-polyAlb as PLT substitutes with normal animals and rabbits with hereditary hyperlipidemia, which are so-called Watanabe rabbits, whether the particles will accelerate pathologic thrombosis, and whether the particles will accelerate or inhibit fibrinolysis.

ACKNOWLEDGMENTS

The authors thank M. Murata, MD, PhD, and K. Yokoyama, MD, PhD, at Keio University for useful discussion about the functional evaluation of H12 peptide.

REFERENCES

1. Blajchman MA. Substitutes and alternatives to platelet transfusions in thrombocytopenic patients. J Thromb Haemost 2003;1:1637-41.
2. Graham SS, Gonchoroff NJ, Miller JL. Infusible platelet membranes retain partial functionality of the platelet GPIb/IX/V receptor complex. Am J Clin Pathol 2001;115: 144-7.
3. Rybak M, Renzulli LA. A liposome based platelet substitute, the plateletsome, with hemostatic efficacy. Biomater Artif Cells Immobilization Biotechnol 1993;21:108-18.
4. Agam G, Livine AA. Erythrocytes with covalently bound fibrinogen as a cellular replacement for the treatment of thrombocytopenia. Eur J Clin Invest 1992;22:105-12.
5. Levi M, Friedrich PW, Middleton S, et al. Fibrinogen-coated albumin microcapsules reduce bleeding in severely thrombocytopenic rabbits. Nat Med 1999;5:107-11.
6. Casals E, Verdaguer A, Tonda R, et al. Atomic force microscopy of liposomes bearing fibrinogen. Bioconjugate Chem 2003;14:593-600.
7. Coller BS, Springer KT, Beer JH, et al. Thromboerythrocytes: in vitro studies of a potential autologous, semi-artificial alternative to platelet transfusion. J Clin Invest 1992;89: 546-55.
8. Takagi J, Petre BM, Walz T, Springer TA. Global comformational rearrangements in integrin extracellular domains in outside-in and inside-out signaling. Cell 2002;110:599-611.
9. Xiao T, Takagi J, Coller BS, Wang JH, Springer TA. Structural basis for allostery in integrins and binding to fibrinogen-mimetic therapeutics. Nature 2004;432:59-67.
10. Shattil SJ, Hoxie JA, Cunningham M, Brass LF. Changes in the platelet membrane glycoprotein IIb-IIIa complex during platelet activation. J Biol Chem 1985;260:11107-14.
11. Marguerie GA, Plow EF, Edgington TS. Human platelets possess an inducible and saturable receptor specific for fibrinogen. J Biol Chem 1979;254:5357-63.
12. Ruggeri ZM, De Marco L, Gatti L. Platelets have more than one binding site for von Willebrand factor. J Clin Invest 1983;72:1-12.
13. Mustard JF, Packham MA, Kinlough-Rathbone RL. Fibrinogen and ADP-induced platelet aggregation. Blood 1978;52: 453-66.
14. De Marco L, Girolami A, Zimmerman TS. Von Willebrand factor interaction with the glycoprotein IIb/IIIa complex. J Clin Invest 1986;77:1272-7.
15. Hawiger J, Kloczewiak M, Bednarek MA, Timmons S. Platelet receptor recognition domains on the α chain of human fibrinogen: structure-function analysis. Biochemistry 1989; 28:2909-14.
16. Kloczewiak M, Timmons S, Hawiger J. Localization of a site interacting with human platelet receptor on carboxy-terminal segment of human fibrinogen γ chain. Chain Biochem Biophys Res Commun 1982;107:181-7.
17. Takeoka S, Teramura Y, Okamura Y, et al. Fibrinogen-conjugated albumin polymers and their interaction with platelets under flow conditions. Biomacromolecules 2001; 2:1192-7.
18. Takeoka S, Teramura Y, Ohkawa H, Ikeda Y, Tsuchida E. Conjugation of von Willebrand factor-binding domain of platelet glycoprotein Ibα to size-controlled albumin microsheres. Biomacromolecules 2000;1:290-5.
19. Teramura Y, Okamura Y, Takeoka S, et al. Hemostatic effects of polymerized albumin particles bearing rGPIa/IIa in thrombocytopenic mice. Biochem Biophys Res Commun 2003;306:256-60.
20. Takeoka S, Teramura Y, Okamura Y, et al. Rolling properties of rGPIbα-conjugated phospholipid vesicles with different membrane flexibilities on vWf surface under flow conditions. Biochem Biophys Res Commun 2002;296:765-70.
21. Kitaguchi T, Murata M, Iijima K, et al. Characterization of liposomes carrying von Willebrand factor-binding domain of platelet glycoprotein Ibα: a potential substitute for platelet transfusion. Biochem Biophys Res Commun 1999; 261:784-9.
22. Nishiya T, Murata M, Handa M, Ikeda Y. Targeting of liposomes carrying recombinant fragments of platelet membrane glycoprotein Ibα to immobilized von Willebrand factor under flow conditions. Biochem Biophys Res Commun 2000;270:755-60.
23. Nishiya T, Kainoh M, Murata M, Handa M, Ikeda Y. Reconstitution of adhesive properties of human platelets in

liposomes carrying both recombinant glycoproteins Ia/IIa and Ibα under flow conditions: specific synergy of receptor–ligand interactions. Blood 2002;100:136-42.
24. Okamura Y, Maekawa Y, Teramura Y, et al. Hemostatic effects of phospholipid vesicles carrying fibrinogen γ-chain dodecapeptide in vitro and in vivo. Bioconjugate Chem 2005;16:1589-96.
25. Wertheimer E, Shapiro B, Fodor-Salomonowicz I. Stability of fibrinogen in normal and pathological plasma. Br J Exp Pathol 1944;25:121-5.
26. Kloczewiak M, Timmons S, Lukas TJ, Hawiger J. Platelet receptor recognition site on human fibrinogen. Synthesis and structure-function relationship of peptides corresponding to the carboxy-terminal segment of the γ chain. Biochemistry 1984;23:1767-74.
27. Kloczewiak M, Timmons S, Bednarek MA, Sakon M, Hawiger J. Platelet receptor recognition domain on the γ chain of human fibrinogen and its synthetic peptide analogues. Biochemistry 1989;28:2915-9.
28. Lam SC, Plow EF, Smith MA, et al. Evidence that arginyl-glycyl-aspartate peptides and γ chain peptides share a common binding site on platelets. J Biol Chem 1987;262: 110-5.
29. Hallahan DE, Geng L, Cmelak AJ, et al. Targeting drug delivery to radiation-induced neoantigens in tumor microvasculature. J Control Release 2001;74:183-91.
30. Takeoka S, Okamura Y, Teramura Y, et al. Function of fibrinogen γ-chain dodecapeptide-conjugated latex beads under flow. Biochem Biophys Res Commun 2003;312:773-9.
31. Okamura Y, Takeoka S, Teramura Y, et al. Hemostatic effects of fibrinogen γ-chain dodecapeptide-conjugated polymerized albumin particles in vitro and in vivo. Transfusion 2005;45:1221-8.
32. Sakai H, Takeoka S, Park SI, et al. Surface modification of hemoglobin vesicles with poly(ethylene glycol) and effects on aggregation, viscosity, and blood flow during 90% exchange transfusion in anesthetized rats. Bioconjugate Chem 1997;8:23-30.
33. Sakai H, Tsai AG, Kerger H, et al. Subcutaneous microvascular responses to hemodilution with a red cell substitute consisting of polyethyleneglycol-modified vesicles encapsulating hemoglobin. J Biomed Mater Res 1998;40:66-78.
34. Klibanov AL, Maruyama K, Torchilin VP, Huang L. Amphipathic polyethyleneglycols effectively prolong the circulation time of liposomes. FEBS Lett 1990;268:235-7.
35. Zalipsky S. Functionalized poly(ethylene glycol) for preparation of biologically relevant conjugates. Bioconjugate Chem 1995;6:150-65.
36. Taub R, Gould RJ, Garsky VM, et al. A monoclonal antibody against the platelet fibrinogen receptor contains a sequence that mimics a receptor recognition domain in fibrinogen. J Biol Chem 1989;264:259-65.
37. Hristova K, Needham D. Phase behavior of a lipid/polymer-lipid mixture in aqueous medium. Macromolecules 1995;28:991-1002.
38. Sou K, Klipper R, Goins B, Tsuchida E, Phillips WT. Circulation kinetics and organ distribution of Hb-vesicles developed as a red blood cell substitute. J Phaemacol Exp Ther 2005;312:702-9.

ADVANCED MATERIALS

DOI: 10.1002/adma.200700661

Ubiquitous Transference of a Free-Standing Polysaccharide Nanosheet with the Development of a Nano-Adhesive Plaster**

Toshinori Fujie, Yosuke Okamura, and *Shinji Takeoka**

Convenient fabrication or manipulation of nanoscale materials will significantly enhance the potential applicability of nanotechnology. One novel methodology for the fabrication of nanoscale materials involving a wide variety of macromolecules is the layer-by-layer (LbL) technique.[1] The LbL method involves alternative adsorption of oppositely charged polyelectrolytes by different non-covalent linking such as electrostatic interactions, hydrogen bonding, or hydrophobic interactions.[1a–d] Application of LbL-based materials has been explored in several fields, such as electrochemical devices, chemical sensors, nanomechanical sensors, nanoscale chemical/biological reactors, and as a drug-delivery system.[2] Nonetheless, potential applications of the LbL method ubiquitously apply to both the liquid and gas phases. Therefore, the ubiquitous manipulation of LbL-based nanocomposites is critical to the development of further functions in nanotechnology.

The LbL method has been applied to the construction of 3D nanocomposites, such as core/shell colloidal particles and hollow capsules.[3] The shells are composed of ultrathin multilayers built on a colloidal core. A hollow capsule is produced by removing the sacrificial template core. Recently, this sacrificial template idea has been applied to the film-fabrication process. Specifically, the LbL method has been used to fabricate a free-standing ultrathin membrane using a spin-coating-assisted LbL (SA-LbL) method.[4] The SA-LbL method can prepare ultrathin membranes by spin-coating each polyelectrolyte alternatively on a substrate covered with a sacrificial layer. Subsequent dissolution of the sacrificial layer releases the free-standing ultrathin membrane within several minutes, unlike conventional protocols that require many hours (e.g., a dipping LbL process). Because the membranes are composed of polymers with a sheetlike structure of nanometer thickness they possess a huge aspect ratio ($\geq 10^6$ depending on the size of the substrate). As such, these structures have been referred to as 'polymer nanosheets' by Miyashita.[5c] The free-standing polymer nanosheets released from the substrate were constructed not only by using the SA-LbL method, but also by using a Langmuir–Blodgett method crosslinking amphiphilic copolymers or by using a sol–gel method with organic–inorganic interpenetrating networks.[5] These polymer nanosheets bearing potential functions that are not available in bulk composites (such as high flexibility and transparency) nanocomposites have been reported to be well-organized, compliant, and robust materials for micro-/nanomechanical studies.[6] However, the polymer nanosheets do not maintain their shape after removal of the substrate and change from having a liquid phase to having a solid outer surface. This limitation is thought to be because the nanosheets with a huge aspect ratio are overwhelmed in the air.

In this communication, we focus on the convenient manipulation of the polymer nanosheet involving ubiquitous transfer from the liquid–solid surface to the air–solid surface using a water-soluble sacrificial membrane. This technique of transferring the polymer nanosheet will also explore the potential advantage of transferring the ultrathin films from the conventional solid substrate to any surfaces that are not always solid interface such as human skin or organs. Therefore, we applied this method to the construction of a new biomedical material called a 'nano-adhesive plaster', consisting of polysaccharides (i.e., a polysaccharide nanosheet) and demonstrated the release of the polysaccharide nanosheet into the human skin.

In order to fabricate the polysaccharide nanosheet, we used chitosan and sodium alginate (Na alginate), which have amino and carboxylic groups as cationic and anionic polyelectrolytes at ambient pH. These polysaccharides are used in biomedical fields as wound dressings and artificial skin because of their biocompatibility and biodegradability.[7] Furthermore, recent studies in LbL assembly using this biopolymer revealed the utility of polysaccharides for biomedical applications such as drug delivery and tissue engineering.[8] Therefore, we selected polysaccharides as the building blocks of the nanosheet. The methodology for the fabrication of the polysaccharide nanosheet utilizes the SA-LbL method as described in the Experimental section. Each polysaccharide was prepared in an aqueous solution containing 0.5 M NaCl in order to weaken the electrostatic interaction between the polyelectrolytes, thereby forming a smooth flat surface.[9] The nanosheet with 10.5 pairs of polysaccharide layers was prepared on a silicon wafer cov-

[*] Prof. S. Takeoka, T. Fujie, Dr. Y. Okamura
Department of Applied Chemistry
Graduate School of Science and Engineering
Waseda University
Tokyo, 169-8555 (Japan)
E-mail : takeoka@waseda.jp

[**] The authors thank Assoc. Prof. Dr. T. Shimamoto at the Consolidated Research Institute for Advanced Science and Medical Care, Waseda University for the technical advice and useful discussions about AFM measurements. This work was supported by the "Consolidated Research Institute for Advanced Science and Medical Care" from MEXT and the Shorai Foundation for Science and Technology (S.T.), Japan. T.F. was the scholar "Doctor-21" of the Yoshida Scholarship Foundation. Y.O. was the recipient of a Research Fellowship from the JSPS for Young Scientists.

ered with an acetone-soluble photoresist sacrificial layer (OFPR-800 LB (200 cP); 2 μm thick, composed of a novolac resin and a photoactive compound). Upon fabrication of the polysaccharide nanosheet, the sacrificial layer was placed in acetone and the transparent nanosheet on the substrate was gradually detached from the edges of the substrate. After 20 min, the polysaccharide nanosheet was fully detached without any shape or size (approximately 4 cm^2) distortion (Fig. 1a). The resulting free-standing nanosheet floating in acetone was then washed by exchanging the acetone three times. This polysaccharide nanosheet was quite stable in acetone or

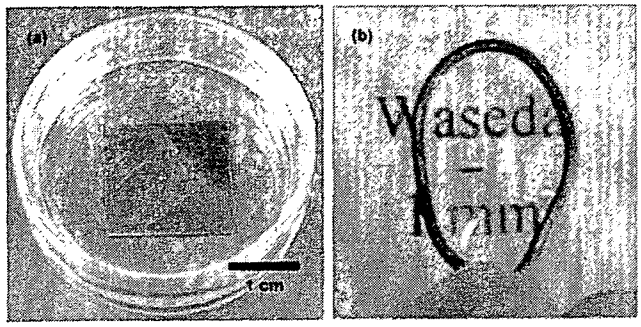

Figure 1. Microscopy image of a polysaccharide nanosheet: a) detached from the substrate and floating in acetone and b) in the air supported by a wire loop.

phosphate buffered saline (PBS, pH 7.4) solution for more than three months. Besides, it could be scooped with a wire loop just as described by Kunitake and co-workers by using a nanosheet consisting of an organic/inorganic interpenetrating network.[5d] Furthermore, no crack was observed in the nanosheet in the air (Fig. 1b). However, once the nanosheet sustained by the wire loop was damaged with a needle, it became ruptured and was immediately ruined. These results demonstrated that the nanosheet could be treated in a dried state provided that it is sustained by a frame. However, its configuration (e.g., shape and size) was restricted by the supporting frame size. Therefore, it was quite difficult to maintain the configuration of the nanosheet in the air without the supporting frame.

A floating nanosheet was put on a calcium fluoride (CaF_2) substrate for characterization of the polysaccharide nanosheet by Fourier transform infrared (FTIR) spectroscopy. By comparing the peaks attributed to the vibration mode among the chitosan hydrochloric acid, Na alginate, and the nanosheet, the main driving force building the nanosheet structure was confirmed to be electrostatic interactions and hydrogen bonding.[10] The asymmetric (band at 1627 cm^{-1}) and symmetric (band at 1523 cm^{-1}) N–H bending vibration modes of non-acylated 2-aminoglucose primary amines derived from the chitosan homopolymer were absent, indicating that the $-NH_3^+$ of the chitosan had reacted with the $-COO^-$ of the alginate by electrostatic interaction. Moreover, the band of the nanosheet at around 3000 cm^{-1}, corresponding to the O–H stretching vibration modes of the polysaccharide structure, became broader than that of the chitosan and alginate homopolymers. This observation suggested intermolecular hydrogen bonding between chitosan and alginate was enhanced over the intramolecular interaction of each homopolymer. Additionally, from the FTIR spectrum of the librated nanosheet, the novolac resin and that of the photoactive compound (diazonaphthoquinone) were barely detected in the nanosheet spectrum compared with the spectrum of the photoresist (thickness: 2.2 μm) directly spin-coated on the CaF_2 substrate. Details of the FTIR spectroscopic study of the nanosheet are given in the Supporting Information.

For the morphological study of the polysaccharide nanosheet surface, the free-standing nanosheet floating in acetone was transferred onto a fresh silicon wafer and observed by using atomic force microscopy (AFM). Large-scale (90 μm × 90 μm) topographic images shown in Figure 2a and b revealed that the nanosheet surface was as smooth and flat as the silicon wafer surface, without any corrugations and wrinkles. These topographical results were obtained because of the high-speed horizontal diffusion of the polymers during spin-coating.[4a] Furthermore, scanning the surface morphology of the polysaccharide nanosheet with a surface profiler in the range of 500 μm showed a significant difference in surface roughness (root-mean squared (RMS) values) of (1.9 ± 0.7) nm (0.5 M NaCl) and (7.1 ± 2.4) nm (0 M NaCl), although a significant difference in the thickness of the polysaccharide nanosheet was not found. Hence, the relatively high ionic strength (0.5 M NaCl) of the polyelectrolyte aqueous solution during fabrication (i.e., using the SA-LbL method) presumably weakened the electrostatic interactions of the polymers, generating a smooth flat surface as the overall morphology of the polysaccharide nanosheet.[9b]

From the cross-sectional analysis of the polysaccharide nanosheet edge, as shown in Figure 2a, the thickness of the nanosheet was estimated to be (30.2 ± 4.3) nm (Fig. 2c). This thickness is in good agreement with that determined for the nanosheet prepared on the substrate ((30.7 ± 4.5) nm), as shown by an ellipsometric analysis (see Supporting Information). Therefore, the thickness of the nanosheet was maintained before and after transference. Because the nanosheet was a LbL film directly assembled on the silicon wafer by 10.5 pairs of the polysaccharides, the thickness of one pair of the polyelectrolytes was calculated to be approximately 2.9 nm. This thickness is in good agreement with that of previously reported LbL films fabricated by the SA-LbL method using similar molecular weight (i.e., ca. 10^5) polyelectrolytes.[4] In addition, the mechanical properties of the polysaccharide nanosheet fabricated in pure water was preliminarily measured by applying air pressure as a bulge test;[5d,6a] the elastic modulus was approximately 1.3 GPa—close to the value of the free-standing polymer nanosheet (1.5 GPa) composed of poly(allylamine hydrochloride) and poly(sodium 4-styrenesulphonate), reported by Tsukruk and co-workers.[5b] (The details of the mechanical properties of the polysaccharide nanosheet are currently under investigation.) Here we

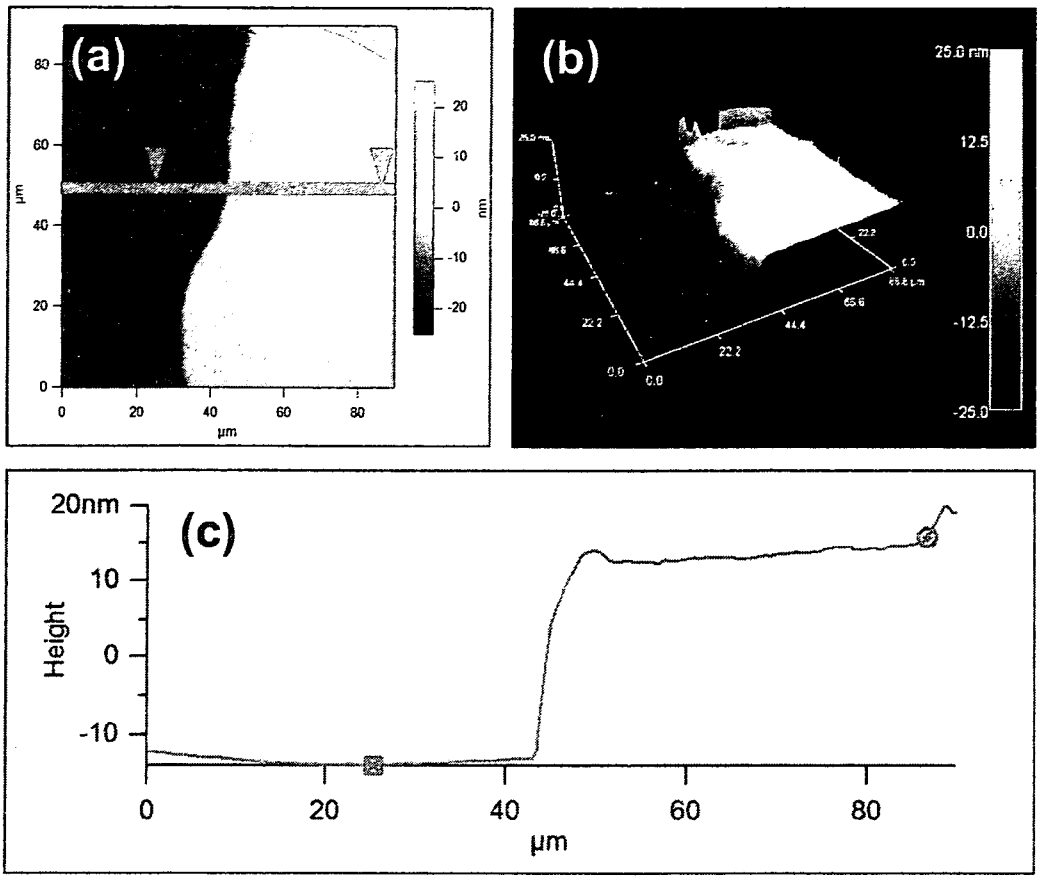

Figure 2. AFM images of the edge of the transferred polysaccharide nanosheet on a SiO_2 substrate: a) top view, b) 3D image, and c) cross-sectional image.

succeeded in the fabrication of a free-standing polysaccharide nanosheet with a high aspect ratio of size and thickness (i.e., $>10^6$).

In order to transfer this polysaccharide nanosheet from the surface of one substrate to another without distorting the overall shape, we incorporated a hydrophilic sacrificial membrane between the polysaccharide nanosheet and the substrate. We named this three-layered composite film a nano-adhesive plaster because we envisaged the nanosheet could attach to skin and the substrate was subsequently peeled off by the dissolution of the sacrificial membrane using water.

The nano-adhesive plaster was prepared by using the method described in the Experimental section (see Fig. 3a). In order to transfer the polysaccharide nanosheet from the substrate onto human skin, we prepared a polyvinyl alcohol (PVA) membrane as a hydrophilic sacrificial membrane. We chose PVA as a suitable material for the sacrificial membrane because it is a water-soluble polymer that does not adversely affect the skin. Owing to its flexibility, silicon rubber was chosen as a substrate for the PVA membrane. The PVA membrane was prepared by spin-coating a 20 wt % PVA aqueous solution on a polypropylene (PP) substrate. The PVA membrane, approximately 1.2 μm thick (measured by surface profiler), was then spontaneously released from the acetone-insoluble PP substrate within a few seconds by immersion in acetone. The free-standing PVA membrane was robust and compliant in acetone when picked up with tweezers. We also tested several flexible polymeric substrates that are insoluble or poorly soluble in acetone, such as polyethylene terephthalate, silicon rubber, and polyvinylchloride. However, PVA was repelled by all of them because of the intermediate hydrophilic–hydrophobic surface of the PP substrate. The free-standing PVA membrane floating in acetone was scooped out and then transferred onto the silicone rubber substrate.

With the resulting PVA–silicone rubber substrate, the polysaccharide nanosheet, modified with a small amount of commercialized luminescent pigment for ease of visibility in the dark, was scooped onto the air–solid surface. As a result, three kinds of free-standing sheets with different thickness were assembled to fabricate the nano-adhesive plaster; silicone rubber on a milliscale (1.0 mm), PVA membrane on a microscale (1.2 μm), and a polysaccharide nanosheet on a nanoscale (30 nm) (Fig. 3b). A luminescent-labeled nanosheet was clearly observed in the dark as a square shape, and no cracks or deformations were observed in the nanosheet over a period of a few months when stored at the ambient

ADVANCED MATERIALS

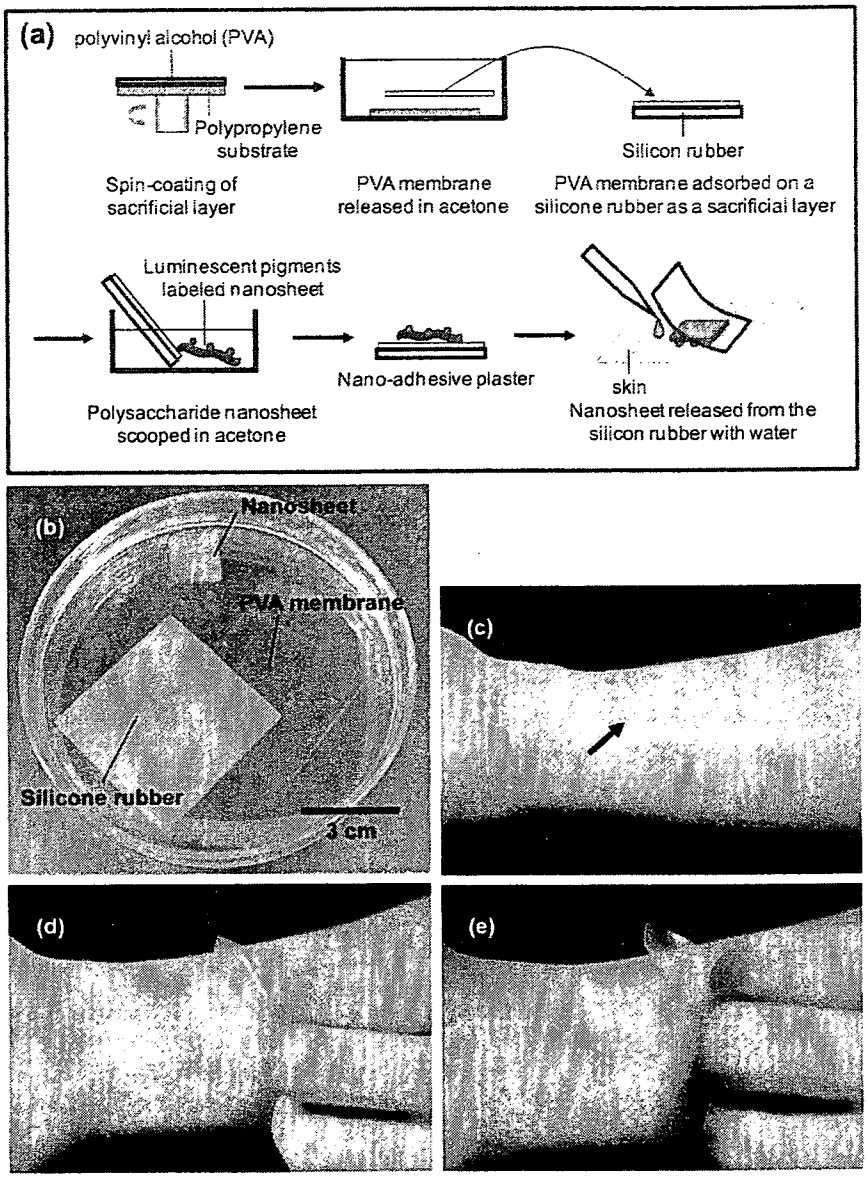

Figure 3. a) Schematic illustration showing the fabrication of a nano-adhesive plaster. b) Three kinds of free-standing sheets floating in acetone, photographed in the dark; the surface of polysaccharide nanosheet was modified with luminescent pigment for ease of visibility. A nano-adhesive plaster on the human skin c) before the polysaccharide nanosheet was released from the silicone rubber and d) after release from the silicone rubber. (e) is the same image as (d) except that it was captured in the dark.

temperature. Although the surface roughness of the PVA membrane was much higher (RMS: (129±98) nm) than that of the polysaccharide nanosheet, any deformation caused by the surface roughness was not found in the polysaccharide nanosheet, suggesting that the polysaccharide nanosheet was stable and fitted on the surface of the PVA membrane with good flexibility. Moreover, the surface roughness of the PVA membrane did not affect that of the polysaccharide nanosheet when the polysaccharide nanosheet was released from the silicone rubber because the PVA membrane was dissolved easily by water.

To test the practical applications of the nano-adhesive plaster, we attached it to the skin on the right arm of a human subject. Prior to transference of the polysaccharide nanosheet from the PVA-silicone rubber substrate onto the skin, the contour on the nanosheet surface was observable because of differences in reflectivity (Fig. 3c arrow). The polysaccharide nanosheet was then released from the PVA-silicone rubber substrate within a few seconds by the dissolution of the PVA layer with a drop of 500 μL deionized (DI) water through a micropipette. The nanosheet on the skin was barely visible from the top view under visible light (Fig. 3d). Luminescent signals from the modified nanosheet confirmed that the shape and size of the polysaccharide nanosheet were preserved on the skin. Furthermore, luminescent regions were barely detected on the removed silicone rubber side, demonstrating the successful transference of the nanosheet onto the skin (Fig. 3e). Moreover, the configuration of the polysaccharide nanosheet was stable for at least 24 h, despite perspiration from the skin and the possibility of it being rinsed away by washing with soap. These results indicated that the polysaccharide nanosheet was released from the silicone rubber by dissolution of the PVA layer with a drop of water and completely transferred onto the skin. The polysaccharide nanosheet was no longer visible on the skin, perhaps because the surface relief of the skin perfectly matched that of the flexible sheet at the nanometer scale. Considering the high biocompatibility and biodegradability of the LbL ultrathin films composed of chitosan and Na alginate reported by some research groups,[11] it is likely that the free-standing polysaccharide nanosheet will be applied in biological systems.

In conclusion, we successfully constructed polymer nanosheets (30 nm thick) comprising the biocompatible and biodegradable polysaccharide-electrolytes with a high aspect ratio of size to thickness (>10^6). Furthermore, we demonstrated transference of the polysaccharide nanosheet from the silicone rubber substrate onto a human skin surface by fabricating a three-layered nano-adhesive plaster. By ubiquitous

transference of the free-standing polymer nanosheet, ultrathin films have been freed from the conventional solid substrate and the advantages of having the films alone at various interfaces, such as human skin, as shown in this report can now be explored. We estimate that the polysaccharide nanosheet would show similar biocompatibility and biodegradability. To our knowledge, this is the first report to show the potential application of free-standing polymer nanosheets in the field of biomedical research. Particularly, the invisible nanosheet on the skin will have obvious applications in the field of skincare. We are currently investigating further the physical and biomedical properties of the polysaccharide nanosheet, such as mechanical strength, biocompatibility, and biodegradability at a cellular level. These results will be reported shortly.

Experimental

The biodegradable polyelectrolytes, chitosan ($M_w = 88$ kDa; 1 Da $= 1.66 \times 10^{-27}$ kg) and sodium alginate (Na Alginate, $M_w = 106$ kDa) were purchased from Nacalai Tesque., Inc. (Kyoto, Japan). OFPR-800 LB photoresist (200 cP) and PVA ($M_w = 22$ kDa) were purchased from Tokyo Ohka Kogyo Co. Ltd. (Kanagawa, Japan) and Kanto Chemical Co., Inc. (Tokyo, Japan), respectively. Silicon wafers purchased from KST World Co. (Fukui, Japan), cut to a size of 20 mm × 20 mm, were immersed in a mixture of sulfuric acid/hydrogen peroxide (3:1) for 10 min and then thoroughly rinsed with DI water (18 MΩ cm). A CaF_2 substrate for FTIR analysis was purchased from Sigma Koki Co., ltd. (Tokyo, Japan). Luminescent pigment was purchased from Sinloihi Co., ltd. (Kanagawa, Japan). Chitosan (1 mg mL^{-1}, 1 % acetic acid, 0.5 M NaCl) and Na alginate (1 mg mL^{-1}, 0.5 M NaCl) solutions were prepared with DI water. All routines for nanosheet fabrication were conducted in a clean room (class 10000 conditions) to avoid contamination.

The free-standing polysaccharide nanosheet was fabricated by using a SA-LbL method as described in the literature [4c]. A 150 μL solution of the polyelectrolyte was dropped onto the substrates and then the substrate was rotated at 4500 rpm for 15 s. Then the substrate was rinsed twice with DI water and dried by spinning (ca. 30 s). The nanosheets were prepared in the following steps (under the above conditions): a) spin-coating the photoresist layer (800 rpm, 3 s and 7000 rpm, 20 s); b) deposition of the chitosan layer (20 min) by physical adsorption; c) repetition of the chitosan and Na alginate multilayering by using the SA-LbL method (4500 rpm, 15 s for each polyelectrolyte); d) termination of the SA-LbL at the chitosan spin-coating stage; e) immersion of the resulting polysaccharide nanosheet adsorbed on the substrate for dissolution of the underlying resist layer in acetone.

For fabrication of a nano-adhesive plaster, a free-standing PVA membrane as a sacrificial layer was prepared by spin-coating (800 rpm, 3 s and 7000 rpm, 20 s) a PVA aqueous solution (20 wt %) onto a PP substrate (5 cm × 5 cm). The PVA layer was released in acetone and transferred onto a piece of flexible silicone rubber. The polysaccharide nanosheet adsorbed on the substrate, before immersion in acetone, was immersed into an aqueous dispersion of commercialized luminescent pigment for 20 min. A small amount of luminescent pigment was present on the surface of the nanosheet. Then the luminescent pigment-labeled nanosheet was released in acetone from the substrate and transferred onto the surface of the PVA-silicone rubber. Sequentially, the nanosheet was transferred onto the human skin by dissolution of the PVA membrane with 500 μL of water.

The polysaccharide nanosheets were photographed using a digital camera OLYMPUS C-5050 ZOOM (Olympus Co., Tokyo, Japan). Surface morphology was observed by using AFM in the tapping mode (MFP-3D-BIO, Asylum Research Co., Santa Barbara, CA). A stokes ellipsometer (Gaertner Scientific Co., Skokie, IL) was also used to measure the thickness of the nanosheet. The wide-range surface roughness of the PVA membrane as well as that of the polysaccharide nanosheets was measured with a surface profiler α-step (KLA-Tencor Corp., San Jose, CA). Characterization of the free-standing nanosheet was confirmed by using a FTIR-410 device (JASCO Corp., Tokyo, Japan).

Received: March 20, 2007
Revised: July 27, 2007

[1] a) Y. Lvov, G. Decher, H. Mohwald, *Langmuir* **1993**, *9*, 481. b) Y. Lvov, K. Ariga, I. Ichonose, T. Kunitake, *J. Am. Chem. Soc.* **1995**, *117*, 6117. c) G. Decher, Y. Lvov, J. Schmitt, *Thin Solid Films* **1994**, *244*, 772. d) V. V. Tsukruk, V. N. Bliznyuk, D Visser, A. L. Campbell, T. J. Buning, W. W. Adams, *Macromolecules* **1997**, *30*, 6615. e) G. Decher, *Science* **1997**, *277*, 1232. f) *Multilayer Thin Films* (Eds: G. Decher, J. B. Schlenoff), Wiley-VCH, Weinheim, Germany **2003**.

[2] a) T. Serizawa, M. Tamaguchi, M. Akashi, *Biomacromolecules* **2002**, *3*, 724. b) L. Zhai, F. C. Cobeci, R. E. Cohen, M. F. Rubner, *Nano Lett.* **2004**, *4*, 1349. c) K. Sano, H. Sasaki, K. Shibata, *J. Am. Chem. Soc.* **2006**, *128*, 1717. d) C. Jiang, V. V. Tsukruk, *Adv. Mater.* **2006**, *18*, 829. e) Z. Tang, Y. Wang, P. Podsiadlo, N. A. Kotov, *Adv. Mater.* **2006**, *18*, 3203.

[3] a) F. Caruso, R. A. Caruso, H. Mohwald, *Science* **1998**, *282*, 1111. b) C. Gao, S. Moya, E. Donath, H. Mohwald, *Macromol. Chem. Phys.* **2002**, *203*, 953.

[4] a) J. Cho, K. Char, J. Hong, K. Lee, *Adv. Mater.* **2001**, *13*, 1076. b) J. Cho, K. Char, *Langmuir* **2004**, *20*, 4011. c) C. Jiang, S. Markutsya, V. V. Tsukruk, *Adv. Mater.* **2004**, *16*, 157.

[5] a) A. A. Mamedov, N. A. Kotov, *Langmuir* **2000**, *16*, 5530. b) C. Jiang, S. Markutsya, Y. Pikus, V. V. Tsukruk, *Nat. Mater.* **2004**, *3*, 721. c) Y. Kado, M. Mitsuishi, T. Miyashita, *Adv. Mater.* **2005**, *17*, 1857. d) R. Vendamme, S. Onoue, A. Nakao, T. Kunitake, *Nat. Mater.* **2006**, *5*, 494. e) H. Endo, Y. Kado, M. Mitsuishi, T. Miyashita, *Macromolecules* **2006**, *39*, 5559. f) S. S. Ono, G. Decher, *Nano Lett.* **2006**, *6*, 592.

[6] a) S. Markutuya, C. Jiang, Y. Pikus, V. V. Tsukruk, *Adv. Funct. Mater.* **2005**, *15*, 771. b) C. Jiang, S. Singamaneni, E. Merrick, V. V. Tsukruk, *Nano Lett.* **2006**, *6*, 2254. c) C. Jiang, M. E. McConney, S. Singamaneni, E. Merrick, Y. Chen, J. Zhao, L. Zhang, V. V. Tsukruk, *Chem. Mater.* **2006**, *18*, 2632.

[7] a) M. N. V. R. Kumar, R. A. A. Muzzarelli, C. Muzzarelli, H. Sashiwa, A. J. Domb, *Chem. Rev.* **2004**, *104*, 6017. b) H. Yi, L. Wu, W. E. Bentley, R. Ghodssi, G. W. Rubloff, J. N. Culver, G. F. Payne, *Biomacromolecules* **2005**, *6*, 2881. c) I. Liao, A. C. A. Wan, E. K. >F. Yim, K. W. Leong, *J. Controlled Release.* **2005**, *104*, 347.

[8] a) T. Serizawa, M. Yamaguchi, M. Akashi, *Biomacromolecules* **2002**, *3*, 724. b) Z. Tang, Y. Wang, P. Podsiadlo, N. A. Kotov, *Adv. Mater.* **2006**, *18*, 3203.

[9] a) S. L. Clark, M. F. Motague, P. T. Hammond, *Macromolecules* **1997**, *30*, 7237. b) J. Cho, H. Jang, B. Yeom, H. Kim, R. Kim, S. Kim, K. Char, F. Caruso, *Langmuir* **2006**, *22*, 1356.

[10] M. G. Sankalia, R. C. Mashru, J. M. Sankalia, V. B. Sutariya, *Eur. J. Pharm. Biopharm.* **2007**, *65*, 215-232.

[11] a) Y. Yang, Q. He, L. Duan, Y. Cui, J. Li, *Biomaterials* **2007**, *28*, 3083. b) A. L. Hillberg, M. Tabrizian, *Biomacromolecules* **2006**, *7*, 2742.

その他